

Higgs Pair Production: Choosing Benchmarks With Cluster Analysis

Martino Dall'Osso^{a,b} Tommaso Dorigo^a Carlo A. Gottardo^a Alexandra Oliveira^{a,b} Mia Tosi^{a,b} Florian Goertz^b

^a*Dipartimento di Fisica e Astronomia and INFN, Sezione di Padova, Via Marzolo 8, I-35131 Padova, Italy*

^b*CERN, 1211 Geneva 23, Switzerland*

ABSTRACT: New physics theories often depend on a large number of free parameters. The precise values of those parameters in some cases drastically affect the resulting phenomenology of fundamental physics processes, while in others finite variations can leave it basically invariant at the level of detail experimentally accessible. When designing a strategy for the analysis of experimental data in the search for a signal predicted by a new physics model, it appears advantageous to categorize the parameter space describing the model according to the corresponding kinematical features of the final state. A multi-dimensional test statistic can be used to gauge the degree of similarity in the kinematics of different models; a clustering algorithm using that metric may then allow the division of the space into homogeneous regions, each of which can be successfully represented by a benchmark point. Searches targeting those benchmark points are then guaranteed to be sensitive to a large area of the parameter space.

In this document we show a practical implementation of the above strategy for the study of non-resonant production of Higgs boson pairs in the context of extensions of the standard model with anomalous couplings of the Higgs bosons. A non-standard value of those couplings may significantly enhance the Higgs pair production cross section, such that the process could be detectable with the data that the Large Hadron Collider will collect in Run 2.

Contents

1	Introduction	1
2	Sampling Signal Kinematics in the Higgs Couplings Basis	3
2.1	Cross Section and Parameter Space Study	4
2.2	Monte Carlo Signal Simulation	7
3	Classification of Final State Kinematics	8
3.1	Two-Sample Tests	8
3.2	The Poisson Likelihood Test Statistic	9
3.3	The Clustering Technique	10
4	Application to Higgs Pair Production	12
4.1	Evolution of Kinematical Sampling Quality with N_{nodes}	12
4.2	Kinematical Sampling with $N_{clus} = 13$	14
4.3	Maps of the Clusters in the Parameter Space	18
5	Conclusions	21

1 Introduction

After the Run 1 discovery of a new scalar particle at 125 GeV [1, 2], which was recognized as the standard model Higgs boson¹, the Large Hadron Collider experiments are now looking forward to the data they will collect in the upcoming Run 2 and in the higher-luminosity phases that will follow. New discoveries are possible with the significantly increased centre-of-mass energy of proton-proton collisions and the foreseen integrated luminosity. The new data will also enable a deep investigation of the 125 GeV particle.

The Standard Model (SM) Lagrangian for the Higgs doublet contains a quartic interaction. When the gauge symmetry of the SM Lagrangian is spontaneously broken, a pattern of masses of the fermions and gauge bosons is generated. Moreover, one additional physical state with cubic and quartic self couplings, the Higgs boson h , is added to the theory. In the SM scenario the strength of all Higgs boson couplings is precisely predicted; deviations from those predictions would thus imply the existence of beyond-standard-model (BSM) physics. A high-statistics study of the couplings of the newly discovered boson may therefore reveal

¹ In this article we follow the terminology which has become standard in high-energy physics, namely we call “Higgs boson” the scalar particle resulting from the Brout-Englert-Higgs (BEH) mechanism when adding a complex doublet of scalar fields to the unbroken standard model Lagrangian. In our analysis we will also relax the doublet assumption.

whether we are in the presence of the last building block of the SM, or rather of the first one of a new physics sector.

The idea of probing BSM physics scenarios (especially the Higgs trilinear coupling) in non-resonant Higgs pair production at proton-proton colliders dates far before the top quark discovery and the LHC design [3]; a large number of studies have been performed since then. After the Higgs discovery, many authors have investigated different phenomenological aspects of the topic (see for example [4, 5, 6, 7, 8, 9, 10, 11, 12, 13, 14, 15, 16, 17, 18, 19]); most of the phenomenology-driven works have focused on the effects of a variation of the Higgs boson trilinear coupling λ . In the present work we consider that any kind of coupling deviation from the SM Higgs sector is a proof that the SM is not complete; therefore all possible Higgs boson couplings should be assumed as BSM parameters. The resulting parameter space is multi-dimensional; its systematic study calls for a principled approach, which we aim to provide here. In this paper we will focus on gluon-gluon fusion (GF) production of Higgs boson pairs, which is the simplest process available to probe the Higgs boson self-coupling at the LHC. The possible BSM deviations in inclusive di-Higgs production arising in other production modes, such as vector-boson fusion [20, 21] or associated production with top quarks (see for example [22]) or vector bosons, probe a different set of parameters in the EFT context. The interpretation of the results of these channels should be studied separately.

Measurements performed by the ATLAS and CMS collaborations with Run 1 LHC data have already started to constrain the value of some of the Higgs boson couplings [23, 24]. Due to interference effects, even small modifications of some of the couplings, within the constraints posed by those measurements, may change drastically the di-Higgs signal topology, and enhance the production cross section enough to make the process accessible with Run 2 data. For that to happen, the observable features of the final state need to be exploited in an optimized way, given the huge cross section of physical processes yielding irreducible backgrounds. This is hard to achieve if one takes the approach of parametrizing the signal cross section in bins of observable final state variables, once the efficiency of a baseline analysis selection is folded in, as one then loses the ability to exploit the signal characteristics and their multi-dimensional densities in an optimal way. We believe it is more promising to identify a manageably small set of benchmark points which are maximally representative of the largest possible volume of a still entirely unexplored parameter space, and to investigate those points in as much detail as possible.

The parametrization we employ in the present work to sample the di-Higgs signal topology is inspired by strongly-coupled theories and assumes the absence of new heavy particles accessible at the LHC energy; we provide it in Section (2). The rest of this work is organized as follows: in Section (3) we describe in detail the technique we devised to determine the similarity of final state densities in the space of observable kinematics, and the clustering procedure which uses that measure of similarity to identify homogeneous regions of parameter space. In Section (4) we describe the application of the technique to determine optimal benchmarks for the study of anomalous di-Higgs production, and we discuss the special features of the resulting partition of the parameter space. We finally draw some conclusions in Section (5).

2 Sampling Signal Kinematics in the Higgs Couplings Basis

In the SM the Higgs boson couplings are exclusively controlled by the particle masses; couplings to light quarks are therefore negligible. Higgs pair production occurs predominantly by gluon fusion via an internal fermion loop, where the top quark is dominant. The extension of this assumption to BSM theories is well motivated if the Higgs sector is minimal (see also [25]). The GF Higgs pair production at the LHC can be generally parametrized with five parameters controlling its tree-level interactions. Written in terms of physical states (equation 2.1) these five parameters are: the Higgs boson trilinear coupling and the top Yukawa interaction, which do exist in the SM Lagrangian and whose deviations are parametrized as multiplicative factors with respect to the predicted SM value (κ_λ and κ_t respectively); as well as the contact interactions with gluons and the contact interaction involving two Higgs bosons, where the latter are interactions genuinely not predicted by the SM that could arise through the mediation of very heavy new states and are parametrized by the absolute couplings c_g , c_{2g} , and c_2 :

$$\mathcal{L}_h = \partial_\mu h \partial^\mu h - \frac{1}{2} m_h^2 h^2 - \kappa_\lambda \lambda_{SM} v h^3 - \frac{m_t}{v} (v + \kappa_t h + \frac{\sqrt{2}}{v} c_2 h h) (\bar{t}_L t_R + h.c.) + \frac{\alpha_s}{\pi v} (c_g h - \frac{c_{2g}}{2v} h h) G^{\mu\nu} G_{\mu\nu}, \quad (2.1)$$

in the case of a linear realization of EWSB $c_{2g} = -c_g$ [26, 27, 28], however low energy corrections could induce a break in this equality even in the linear realization [29].

We assume that Higgs boson couplings to light fermions are negligible, and the absence of any other light state in addition to the SM particles². We also ignore CP violating BSM effects. The different processes contributing to a di-Higgs signal in pp collisions at leading order (LO) are schematized in Fig. 1.

In equation (2.1) we included operators with higher orders of the Higgs boson fields, which are for example a common feature of models where the Higgs doublet is a pseudo-Goldstone boson of a new strong symmetry, and its effective interactions come from field expansions [26, 34]. The translation of this parametrization to the flavour-diagonal Higgs Basis (see [35, 36]) and endorsed by the LHCHXSWG document [37] as a general EFT basis to be used to collider results is trivial; for simplicity we prefer to keep the notation of equation (2.1). Any dimension-6 EFT basis is related to the Higgs basis by analytical relations among the coefficients; an automation of these translations is being developed by [38].

² In the presence of an extended Higgs sector the coupling of the Higgs boson to bottom quarks might be enhanced in the limit of large scalar mixing. The topology of double Higgs production would consequently be modified: besides the presence of a component of the signal initiated by bottom fusion, the gluon-fusion topology would be modified since loop factors would now contain a non-negligible component with a low-mass quark [30]. An enhanced Higgs boson coupling to bottom quarks is not the only physical effect that could arise in SUSY-like theories, where heavy SUSY scalars are predicted (see for example [31, 32, 33]). The non-resonant di-Higgs production in the context of SUSY scenarios is a wide topic and we do not discuss it further in this document.

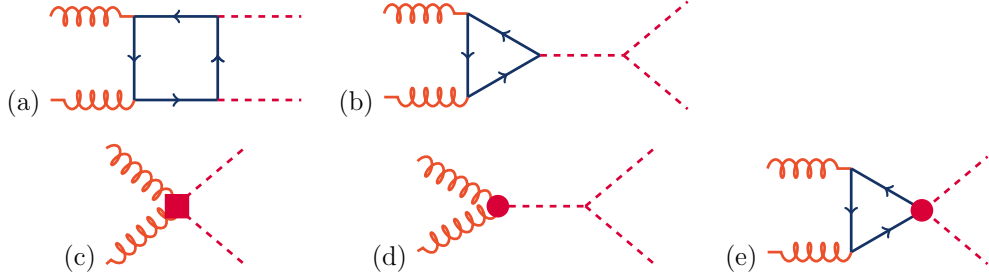


Figure 1. Diagrams of the processes that contribute to Higgs pair production by gluon-gluon fusion at leading order. Diagrams (a) and (b) correspond to SM-like processes, while diagrams (c), (d), and (e) corresponds to pure BSM effects: (c) describes contact interactions between the Higgs boson and the gluons, and (e) exploits the contact interaction of two Higgs bosons with top quarks.

The differential cross section for the full process is proportional to the matrix element squared. Ideally, at any order of radiative corrections we can write the square of the full matrix element (ME) as equation (2.2) below; the various terms in the matrix element expression contribute differently in different regions of the kinematical space:

$$\begin{aligned}
|M_{full}|^2 = & |M_\lambda|^2 + |M_\square|^2 + |M_{c_2}|^2 + |M_{c_g}|^2 + |M_{c_{2g}}|^2 + \\
& (M_\lambda M_\square^\dagger) + (M_\lambda M_{c_2}^\dagger) + (M_\lambda M_{c_g}^\dagger) + (M_\lambda M_{c_{2g}}^\dagger) + \\
& (M_\square M_{c_2}^\dagger) + (M_\square M_{c_g}^\dagger) + (M_\square M_{c_{2g}}^\dagger) + \\
& (M_{c_2} M_{c_g}^\dagger) + (M_{c_2} M_{c_{2g}}^\dagger) + (M_{c_g} M_{c_{2g}}^\dagger) + \text{h.c.}, \tag{2.2}
\end{aligned}$$

Above, M_j identifies the matrix element piece where the parameter j is the representative one, and M_\square corresponds to the box diagram.

2.1 Cross Section and Parameter Space Study

In order to carry out a phenomenological study we need first to define the range of parameters variation we want to consider. Some of the parameters relevant to the production phase are completely unconstrained by single Higgs boson measurements: among them are the triple Higgs coupling and the di-Higgs contact interactions with top quarks and gluons. Others, such as the top Yukawa coupling, are already constrained by experimental results [23, 24]. A precise interpretation of all experimental bounds on the effective operators and their effect on the considered process is not trivial, as the parameters do not only affect the predicted rate of di-Higgs production, but also the kinematics of the final state.

The single Higgs boson production measurements performed so far at the LHC constrain the κ_t and c_g parameters. The combination of the single Higgs results using the κ formalism [39] shows that by marginalising over all other Higgs couplings the allowed values

of κ_t are constrained at 95% C.L. in the region between 0.5 and 2.5. A Bayesian analysis of BSM operators also based on available Higgs results constrains the c_g parameter to be at most at the $O(10^{-1})$ level [40, 41, 42, 43]. The other parameters are constrained only by absolute cross section limits on inclusive di-Higgs production [44]. The theoretical range of validity is to some extent "model" dependent, for example, in a linear dimension six realization will depend on what is the cutoff scale.

The full cross section of the GF di-Higgs production can be written as a polynomial in terms of all the model parameters as in equation (2.3) below:

$$\frac{\sigma_{hh}}{\sigma_{hh}^{SM}} = \left(\begin{aligned} &A_1 \kappa_t^4 + A_2 c_2^2 + (A_3 \kappa_t^2 + A_4 c_g^2) \kappa_\lambda^2 + A_5 c_{2g}^2 + (A_6 c_2 + A_7 \kappa_t \kappa_\lambda) \kappa_t^2 \\ &+ (A_8 \kappa_t \kappa_\lambda + A_9 c_g \kappa_\lambda) c_2 + A_{10} c_2 c_{2g} + (A_{11} c_g \kappa_\lambda + A_{12} c_{2g}) \kappa_t^2 \\ &+ (A_{13} \kappa_\lambda c_g + A_{14} c_{2g}) \kappa_t \kappa_\lambda + A_{15} c_g c_{2g} \kappa_\lambda \end{aligned} \right) \quad (2.3)$$

The state-of-the-art calculations for the di-Higgs cross section in the SM combine effective techniques in treatment of NNLO QCD corrections and top mass and width effects. In proton-proton collisions at 13 TeV the prediction is $\sigma_{hh}^{SM} = 34.3 \text{ fb} \pm 9\% \text{ (scale)} \pm 2\% \text{ (PDF)}$, while at 8 TeV it is $\sigma_{hh}^{SM} = 9.96 \text{ fb} \pm 10\% \text{ (scale)} \pm 2\% \text{ (PDF)}$. Those values are based on the recent progresses of [45, 46], using the CT10 PDF set [47] and use as input the mass values $m_h = 126 \text{ GeV}$, $m_t = 173.18 \text{ GeV}$ and $m_b = 4.75 \text{ GeV}$. Regarding dimension six parametrization the state-of-the-art calculations are made in [51].

At LO the scattering amplitude for the $gg \rightarrow hh$ process contains terms with different loop structures, corresponding to the different BSM operators. Therefore one can imagine that real jet emissions at next-to-leading order in QCD could yield significantly more complex topologies with respect to the LO predictions. The complications could depend on the microscopic nature of the interaction, i.e. on whether the matrix amplitude in a given parameter space point is dominated by box-like, by triangle-like or by point-like interactions. The real emissions for the $gg \rightarrow hh$ process are not trivial to compute; the relative diagrams would contain up to pentagons to be matched with parton showers. Different groups of phenomenologists are progressing in the calculation of (two-loop) NLO predictions matched to shower level effects for the GF di-Higgs process, especially for the SM case; see for example [46, 48, 49]. In the case of the SM, the shape of high- p_T tail of the di-Higgs boson system is mis-modeled by the Monte Carlo by about 10% including top mass effects [46, 50].

We simplify the parameter space mapping in the limit of the present calculational capability in BSM assuming that each of the matrix element pieces of equation (2.2) be equivalent to the use of an overall k-factor, as written in the first equality of equation (2.4). As a second step we make the stronger assumption that the k-factors related to the different ME pieces are equal, and that they may be taken as a k-factor derived for the SM case, leading to the second equality in equation (2.4):

$$(M_i M_j^\dagger + h.c.)^{\text{higher order}} = k_{ij} (M_i M_j^\dagger + h.c.)^{LO} = k_{SM} (M_i M_j^\dagger + h.c.)^{(LO)}, \quad (2.4)$$

the above approximations are expected to be good for QCD-like radiative corrections when quoting the total cross section. The enhancement in total cross section due QCD NLO corrections is mainly due to soft gluon radiation from initial state [51]. For a characterization of the differential distributions, on the other hand, the one above might not be an entirely satisfactory description; yet we use it here as it will facilitate the mapping of experimental results derived with LO simulations to the results of a radiative corrected calculations. Using the approximation (2.4) it is possible to calculate the coefficients of the polynomial (2.3) by interpolating the results of LO computations in different points of parameter space. The values corresponding to the coefficients of the cross section for LHC proton-proton collisions at 13 TeV are in table (1). Those were derived with the Monte Carlo simulation described in the next section.

A1 = 2.12	A2 = 1.30	A3 = 0.30	A4 = 16.3	A5 = 192.4
A6 = -3.07	A7 = -1.42	A8 = 1.04	A9 = 7.61	A10 = 15.44
A11 = -8.63	A12 = -23.0127	A13 = 4.54	A14 = 9.38	A15 = 225.44

Table 1. Coefficients of equation (2.3) for LHC proton-proton collisions at 13 TeV.

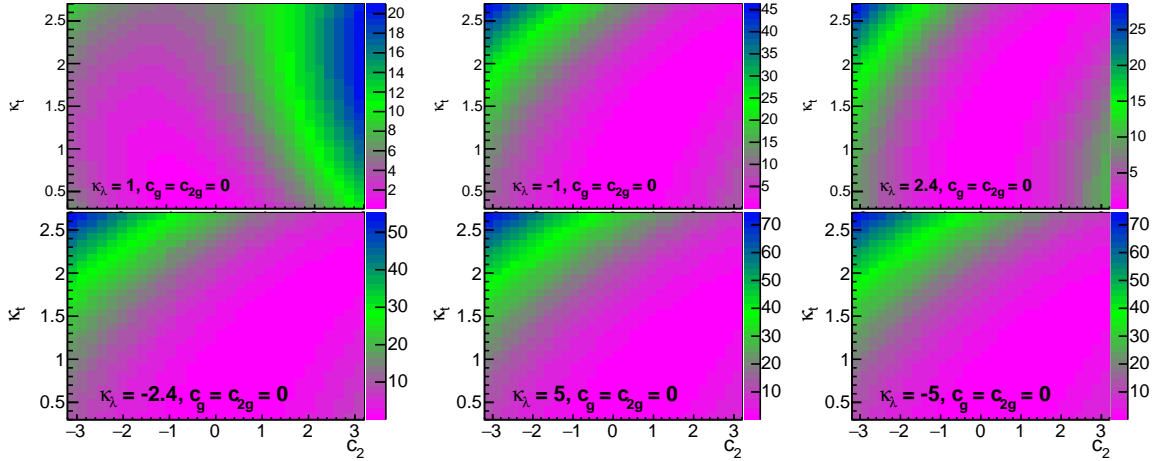


Figure 2. Cross section enhancements (σ_{BSM}/σ_{SM}) in selected slices of parameter space. Left and center columns: the plane $k_t : c_2$ for selected values of k_λ and $c_g = c_{2g} = 0$. Right: the plane $c_g : c_{2g}$ for selected values of k_t , k_λ , and c_2 .

In general, BSM theories do not provide a unique prediction for the Higgs boson trilinear coupling. The current experimental limit on non-resonant di-Higgs production in the SM comes from the study of the $\gamma\gamma b\bar{b}$ and $4b$ final states at 8 TeV by ATLAS [44, 52]. Those are respectively $\sigma_{hh \rightarrow \gamma\gamma b\bar{b}}^{SM} < 5.72$ fb (220 times the SM value) and $\sigma_{hh \rightarrow 4b}^{SM} < 202$ fb (62.4 times the SM value). Both results were derived by counting experiments and therefore without strong assumptions on the signal topology in the final state other than the presence of two Higgs bosons.

Considering the ATLAS SM results extended to all parameter space we find the $|\kappa_\lambda|$ -

only variation to be constrained in the region $|\kappa_\lambda| \simeq 20$ ³. Following a similar approach the c_2 parameter is constrained to $|c_2| < 5$ at 95% CL when $\kappa_\lambda = 1$ and $\kappa_t \in [0.5, 2.5]$.

A cursory look at the kinematics of the final state, as described in any of the already mentioned phenomenological references, suggests that different choices of the coupling parameters give rise to quite varied density functions for the observable kinematics. This convinces us of the need of a systematic approach to characterize the signal topology. The method we propose to perform such a study is described in Section (3).

2.2 Monte Carlo Signal Simulation

The simulation setup was produced by the authors of [53]. The LO process is already at one-loop level, in the approach followed in [53] the loop factors are calculated on an event-by-event basis with a **Fortran** routine on top of an *aMC@NLO* [54, 55] effective model. The NN23L01 PDF set [56] was used. Those simulations represent the state-of-the art in the description of BSM di-Higgs production.

In order to retain generality of the results of our clustering technique to any di-Higgs final state, and invariant to further analysis cuts and/or analysis techniques, we study the event topology as it results from the production of the two Higgs bosons before any subsequent decay or final-state radiation effect; no generation cut is applied to the processes. For each studied point of the parameter space we generate 20,000 events for proton-proton collisions at 13 TeV center-of-mass energy. These are sufficient for the task of understanding how the event kinematics varies as a function of the model parameters.

The process we are considering is a $2 \rightarrow 2$ process at leading order. The two Higgs bosons are produced with identical transverse momenta, and they are perfectly back-to-back in azimuth. The final state can then be completely defined by just three kinematical variables, if we ignore the irrelevant azimuthal orientation of the bosons. Furthermore, one of the three variables can be used to isolate all the information related to the PDF of the colliding partons, which is also irrelevant to the physics of the production process once one focuses on a specific initial state (the gluon-gluon fusion process); this can be taken as the magnitude of the boost of the centre-of-mass frame as seen in the laboratory frame.

The two remaining variables, which provide direct information on the physics of GF di-Higgs production, can be chosen to be the invariant mass of the di-Higgs system (m_{hh}) and the modulus of the cosine of the polar angle of one Higgs boson with respect to the beam axis ($|\cos\theta^*|$). Since we are using parton level information, this last variable is equivalent to the polar angle in the Collins-Soper frame ($|\cos\theta_{CS}^*|$) [57], which is commonly used in experimental analysis. In this work we will rely on m_{hh} and $|\cos\theta^*|$ to characterize the final state kinematics produced by different choices of the value of anomalous Higgs (self-)coupling parameters.

³The κ_λ parameter is a multiplicative variation of a small value ($\lambda_{SM} \sim 0.13$), therefore an $O(10)$ variation would not affect the calculational validity of the perturbative approach.

3 Classification of Final State Kinematics

The choice of benchmarks for the study of a new physics model is usually arbitrary, as it obliges to several partly conflicting desires. While the collection of benchmarks should in principle offer an exhaustive representation of the varied final state composition and topologies that the new physics model may give rise to, one's choice of the specific values of the model parameters to study in more detail falls on those which are within the sensitivity reach of a specific amount of data collected by a given experiment at a given time. In that case the focus is usually on the cross section of the new physics signal, which is identified as the most important factor. As it happens with the drunkard who lost his watch in the dark and only searches it under the street lamps, this approach is guaranteed the highest short-term impact but is not very systematic.

The case of Higgs pair production at the LHC offers a peculiar situation, as in the short term we will be unable to achieve experimental sensitivity to the largest part of the BSM parameter space. Furthermore, anomalous Higgs pair production processes are characterized by a final state which is homogeneous in its composition, as opposed to, e.g., Supersymmetric production processes, which give rise to a quite rich and diverse possibility of different final states depending on the exact choice of theory parameters. Within that homogeneous final state, anomalous di-Higgs production processes offer quite varied kinematics as a function of the model parameters. This makes it an ideal ground for a principled and quantitative approach to the choice of benchmark points.

In light of the above considerations, we take the problem from the side of shape information rather than normalization. By identifying sets of parameters which yield similar final state kinematics we simplify the problem of investigating a large and unconstrained model space. The resulting partition of the space will remain useful as the integrated luminosity collected by the LHC experiments grows from tens to hundreds of inverse femtobarns.

The task of partitioning the parameter space into homogeneous regions can be performed with cluster analysis techniques. These allow the grouping of elements of a set into subsets in such a way that members of each subset are mutually more similar to one another than are elements belonging to different subsets. The similarity will, in our case, be described by an ordering parameter which is constructed with the event kinematics, employing the techniques of hypothesis testing.

3.1 Two-Sample Tests

In order to define a metric to classify physics models based on the similarity of the event kinematics they describe in the feature space, we need to choose a general statistical framework as well as a suitable two-sample test statistic. At first, we might consider the problem as one of hypothesis testing. We would consequently define a test size α and a null hypothesis H_0^{ij} for each pair of parameter space points i and j , the null hypothesis being that the corresponding data samples S_i and S_j share the same parent probability density function –or, in other words, that models i and j describe the same physics. The choice of a test statistic and its evaluation on the pair of samples S_i , S_j would then allow us to populate a

matrix describing the mutual compatibility of the samples, in the form of a set of pass/fail bits. Clearly, such a result would not be practical for the task of grouping samples into subsets of similar characteristics. Furthermore, it must be noted that as we start with samples which do originate from distinguishable parameter space points and which yield different density functions, it is only the lack of infinite statistics what would prevent us from calling two samples passing the test as “different” from an experimental point of view. We may turn the limited statistics of the datasets to our advantage if we realize that what we need is an analog answer rather than a digital one: a degree of similarity between each pair of samples must take the place of the yes/no answer of the hypothesis test. To the extent that we test samples of 20,000 events (see Section 2.2), we can discern significant differences only among some of them. A test statistic (TS) such as a χ^2 probability or a likelihood value may be used to determine which samples should be grouped into homogeneous subsets.

There exist a large variety of two-sample tests that may be used for the task at hand. To name a few, one may use the Anderson-Darling test, the Kolmogorov-Smirnov test, the χ^2 test, the T test, or others. The ones mentioned above are usually single-dimensional tests, in the sense that they are meant to compare two single-dimensional distributions; their extension to multi-dimensional data is not always straightforward, as it is subject to implementation choices that call for detailed power studies⁴. In a multi-dimensional setup possible choices also include the Energy test [58] or nearest-neighbour-based metrics. Such unbinned multi-dimensional TS may be the right choice in situations when the statistics of the samples to be compared are very small, or when the dimensionality of the problem is large. In the specific case of non-resonant di-Higgs production, however, we found that the TS with highest power to detect localized differences in the kinematic distributions is a simple log-likelihood function based on Poisson counts in a set of 2-dimensional bins. That is the solution we investigate and discuss in this work.

3.2 The Poisson Likelihood Test Statistic

In the specific application described here, the numerosity of our generated datasets (20,000 events per sample) and the small dimensionality of the feature space that completely defines the final state of the process allow us to employ as test statistic a simple log-likelihood function constructed as a product of $N_{bin}^{tot} = 50 * 5$ Poisson terms. The number of bins in m_{hh} and $|\cos\theta^*|$ are chosen such that the main kinematic features of the distribution are properly modeled while retaining sufficiently populated bins. We found appropriate for our application to have fifty 30-GeV-wide bins in m_{hh} in the range from zero to 1500 GeV and five 0.2-wide bins in $|\cos\theta^*|$ from zero to one.

The TS is constructed by considering that if two samples come from the same prior distribution, then the maximum likelihood estimate for the expected contents in a given bin i , which the two samples populate respectively with $n_{i,1}$ and $n_{i,2}$ entries, is $\hat{\mu}_i =$

⁴The power of a test $1 - \beta$ is the probability that the test is capable of evidencing the truth of the alternative hypothesis, as β is the type-2 error rate, *i.e.* the probability that the test rejects the alternative hypothesis when in fact it is the true one.

$(n_{i,1} + n_{i,2})/2$. One may then write, for the probability to observe $n_{i,1}$ and $n_{i,2}$ event counts in bin i from the two samples S_1 and S_2 ,

$$p\left(n_{i,1}, n_{i,2} \mid \mu_i = \frac{n_{i,1} + n_{i,2}}{2}\right) = e^{-2\mu_i} \frac{\mu_i^{-n_{i,1}-n_{i,2}}}{n_{i,1}!n_{i,2}!} \quad (3.1)$$

For the two samples the log-likelihood can then be written as

$$TS = \log(L)_{12} = \log \Sigma_{i=1}^{N_{bin}^{tot}} [-2\mu_i - (n_{i,1} + n_{i,2})\log\mu_i - \log(n_{i,1}!) - \log(n_{i,2}!)] \quad (3.2)$$

The above TS is particularly sensitive to small-scale features of the distributions under test, and is thus well suited to our task as we are confronted with samples exhibiting bimodal structures in the studied spectra (see for instance Fig. 5). In contrast, TS which are more sensitive to large-scale structure may give precedence to the latter when used as an ordering parameter in a clustering procedure: we have observed that such behaviour gives rise to unwanted results, whereby bimodal and single-modal distributions are clustered together.

3.3 The Clustering Technique

The log-likelihood TS described above can be directly used as an ordering parameter to perform a cluster analysis. This is due to the equivalence of the TS to a likelihood ratio where the numerator is the TS itself and the denominator is a “saturated model” where the two distributions S_i and S_j are identical, and the possibility to interpret the ratio as a χ^2 statistic providing a goodness-of-fit value [59, 60]. In other words, the values $\log L_{ij}$ and $\log L_{kl}$ obtained respectively by testing the compatibility of samples ij and kl are suitable to determine *e.g.* if samples S_i and S_j are more similar to each other than are samples S_k and S_l : this is the case if $\log L_{ij} > \log L_{kl}$ ⁵.

The clustering procedure must use the TS in an iterative way, producing a grouping of the parameter space points based on the kinematic densities of the corresponding final states. Such a task can be performed in a number of ways, yielding in general different results. The algorithm we chose matches our desire to create *homogeneous* regions of parameter space based on the TS metric, and it allows to univocally identify the sample in each cluster which is the most representative of the set - what we call a *benchmark*. The benchmark is chosen as the sample which is the most similar to all the other samples associated to the same cluster.

The sample comparisons are pairwise, therefore we can form $N_{sample}(N_{sample} + 1)/2$ two-sample-test results as described above. We define the following procedure to group all the samples into a given number of clusters (N_{clus}):

⁵For a generic test statistic which is not distribution-independent, this is not granted; one is then forced to study the probability density function under the null hypothesis of the TS for each pair of tested distributions, comparing p -values derived from tail integrals of the TS. Besides being extremely CPU consuming, this also requires to use part of the data to construct the null distribution of the TS for each sample pair.

1. Start by identifying each of the N_{sample} sets as one-element clusters.
2. Define the cluster-to-cluster *similarity* as $TS^{min} = \min_{ij}(TS_{ij})$, where i runs on all elements of the first cluster and j runs on all elements of the second cluster.
3. Find among all the possible pairs of clusters the two with the highest value of TS^{min} ; merge the two clusters into one, and recompute the resulting benchmark.
4. Repeat step 3 above until N_{clus} clusters are left, keeping a record of all intermediate results.
5. Identify the benchmark sample in a cluster as the element k with the highest value of $TS_k^{min} = \min_i(TS_{ki})$ between the clustered samples, where i runs on all elements of the cluster except k (if more elements have the same value of TS_k^{min} , one may by convention take the first one).

Figure 3 describes graphically the clustering method. For any given choice of the number of clusters the procedure returns the optimal clustering and the benchmark in each cluster. Of course, this implies that there is a trade-off between intra-cluster homogeneity and N_{clus} : as the latter decreases, more and more discrepant elements are clustered together; accordingly, the benchmark becomes less and less representative on the whole of the subset that contains it.

It is easy to see how the technique outlined above possesses some attractive features for our application. There is always a well-defined benchmark in each cluster, and the criterion by which points are clustered together privileges a maximum intra-cluster uniformity over an average one. In the next section we apply the method to the parameter space points describing BSM di-Higgs production, which allows us to show what those properties mean in practice.

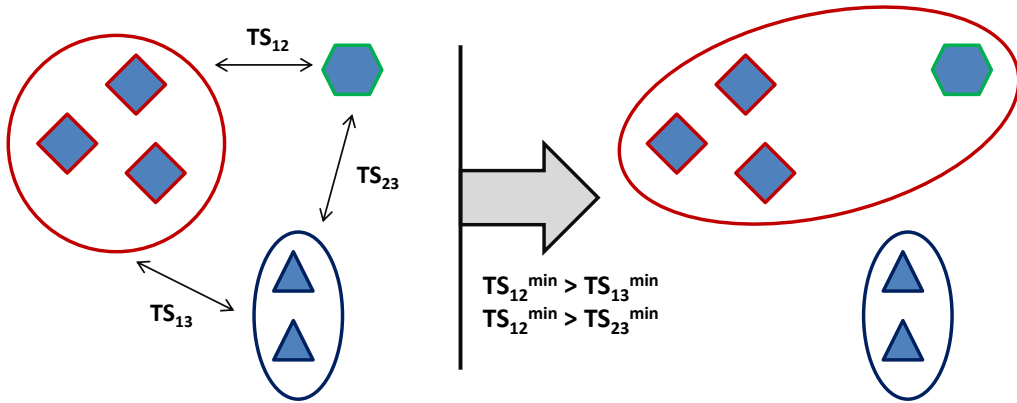


Figure 3. Graphical description of the clustering procedure.

4 Application to Higgs Pair Production

In this Section we discuss the application of the procedure described in Section (3) to GF di-Higgs production at the LHC. The first step is to identify the set of parameter space points on which we wish to run the cluster analysis. Ideally one would like to start with a regular and homogeneous grid in the five-dimensional parameter space of anomalous couplings described in Section (2); however any meaningfully-spaced regular grid would require a prohibitive number of simulated data samples. Instead of using a regularly spaced grid, we focus primarily on the regions of parameter space where the probability densities of the final state observables exhibit the fastest variability with parameter variation. These regions coincide with local minima of the production cross section, as is discussed below, in Section (4.3). The resulting somewhat arbitrary population of the five-dimensional grid is seen *a posteriori* to be able to picture reasonably well the resulting topologies. It includes 1438 points of the five-dimensional parameter space, composed by the following three sets:

- A purely three-dimensional grid of points in the hyperplane defined by $c_g = c_{2g} = 0$, which is described by the parameters κ_λ , κ_t , and c_2 . The grid contains 636 parameter space points, scattered within a 3D region whose boundaries are described in Section (2.1); an increased density of points is allocated near the point corresponding to the SM hypothesis. The points are identified by combinations of the following parameter values: $\kappa_\lambda = \pm 1, \pm 2.4, \pm 3.5, \pm 5, \pm 7.5, \pm 10, \pm 12.5, \pm 15$; κ_t from 0.5 to 2.5 in steps of 0.25; c_2 between -3.0 and 3.0 in steps of 0.5.
- The above 3-dimensional parameter sampling is extended to include Higgs-gluon contact interactions with the primary goal of understanding how different kinematic structures are generated by the addition of different Lorentz structures in the ME. We start with a geometrically well-spaced grid in the three dimensions, identified by values of $\kappa_\lambda = 1, \pm 2.4, \pm 5, \pm 10, \pm 15$, with the addition of some points at $|\kappa_\lambda| = 3.5$; values of κ_t from 0.5 to 2.5 in steps of 0.5; and all the integer values of c_2 between -10.0 and 10.0 ⁶. For each of these points the pair of c_g and c_{2g} values (both constrained to be < 1) which minimizes the cross section is selected. Parameter space points which yield a cross section exceeding $100 * \sigma_{SM}$ are rejected.

4.1 Evolution of Kinematical Sampling Quality with N_{nodes}

The total number of required clusters N_{clus} , and therefore the total number of regions into which the parameter space is divided, is the only free parameter in the clustering procedure described in Section (3). Figure (4) is a pictorial diagram of how the different parameter space points, already subjected to a grouping into 20 clusters, are further clustered together when N_{clus} decreases from 20 to 2.

The uniformity of the kinematical distributions within each cluster is a qualitative criterion which can be used to choose the target value of N_{clus} . A large number of clusters

⁶Note that the predictions at the boundaries of the parameter space, i.e., at very large values of the couplings, should be taken with a grain of salt.

provides a finer sub-division of the parameter space and improves the uniformity of the kinematic distributions within each cluster. In our specific application we have observed that for $N_{clus} > 13$ the differences between the kinematical distributions of the samples included in different clusters are too small to be exploitable by data analysis. Furthermore, a too large number of benchmarks puts a heavy load on the experimental treatment of the data to probe the full parameter space. On the other hand, when N_{clus} becomes smaller than 10 or so, samples grouped within the same cluster exhibit marked differences, such that the corresponding benchmark does not appear suitable to accurately represent their behaviour.

We may examine how the clustering procedure works by following the evolution of the cluster which contains the parameter space point corresponding to the SM as the value of N_{clus} varies. The relative distributions are shown in Fig. (4), in which the SM sample (blue) is compared with the cluster benchmark (red) and with the other elements of the same cluster (brown). For brevity we only show the m_{hh} distribution, which is the variable carrying the largest amount of information. By examining the figure it is evident that for $N_{nodes} = 13$ or greater the SM sample is well described by the corresponding benchmark, as are the other samples in the cluster.

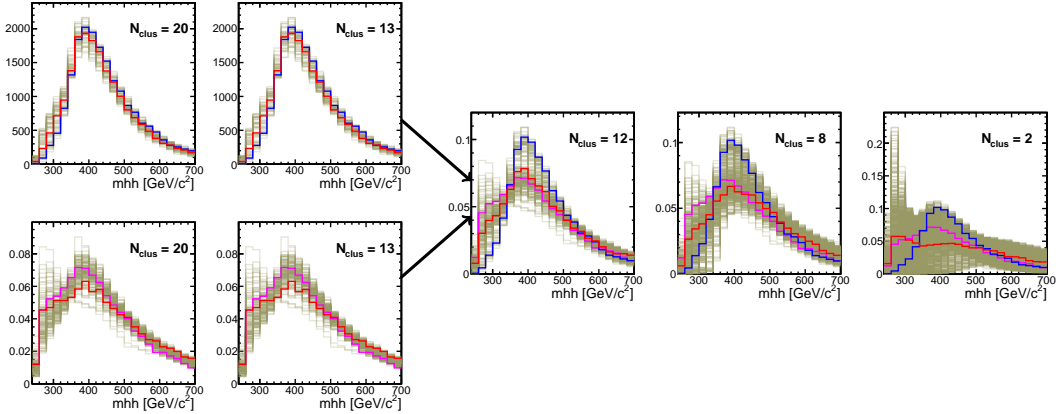


Figure 4. Distribution of the invariant mass of the Higgs boson pair for samples grouped in a single cluster, for different values of N_{clus} . The red distribution is the cluster benchmark, the blue is the SM sample, the magenta corresponds to the point ($\kappa_\lambda = -7.5$, $\kappa_t = 0.5$, $c_2 = -3$ and $c_g = c_{2g} = 0$) and brown are the other samples in the cluster. The clusters splitting when $N_{nodes} = 12$ is increased to $N_{nodes} = 13$ is highlighted.

When assessing the degree of homogeneity of the distributions shown in the figures, one should bear in mind that the choice operated here for the number of clusters ($N_{clus} = 13$) is aimed at obtaining a reasonable trade-off between homogeneity and numerosity; in operating this choice we followed the guideline of offering to experimental collaborations a manageable number of different models for an initial study, appropriate for the integrated luminosity that the LHC will deliver in the next few years; we also paid special attention

to the cluster which includes the sample corresponding to the SM point, as that parameter space point is of course of special interest. As the di-Higgs mass resolution is detector-dependent as well as final-state dependent, and the discernible and statistically significant features presented by a possible signal depend on the amount of investigated integrated luminosity, the choice of the most appropriate number of clusters (with a corresponding different homogeneity in the intra-cluster kinematical distributions) should in general be informed by those conditions.

It should be noted that, although the main purpose of the clustering of parameter space points and the identification of benchmarks described in this Section is to provide the experimental collaborations with an initial choice for BSM theories to be studied in detail with LHC Run 2 data, the grouping of parameter space points we provide does allow one to extend results of an experimental search performed on a benchmark point to all other points of the cluster which contains it, without a large hit in performance of the analysis. In a separate study, which we do not report here for brevity, we have assessed the degree of validity of upper limits on the signal cross section derived for model points included in a cluster by extrapolating the upper limit obtained for the corresponding benchmark point. An assessment of the systematic uncertainties related to that extrapolation may then allow one to easily derive upper limits in wide regions of the parameter space based on the results obtained for the benchmarks.

4.2 Kinematical Sampling with $N_{clus} = 13$

The cluster analysis described above allows us to divide the parameter space into regions wherein the kinematics of the final state is homogeneous. In each region a benchmark is identified as the sample which better represents that cluster, namely the element k with the highest value of $TS_k^{min} = \min_i(TS_{ki})$ between the clustered samples, where i runs on all elements of the node except k , as described in Section (3.3).

The parameter space values of the benchmarks obtained with $N_{clus} = 13$ are listed in Table (2). The benchmarks distribute rather evenly in the space of model parameters, without concentrations in specific corners of phase space; furthermore, both samples with and without Higgs-gluon contact interaction are represented in the set. The first cluster includes the SM point, and shows an excellent homogeneity among all the included elements. Cluster 2 includes the sample with the maximal interference between the Lagrangian contributions, as shown by the characteristic doubly peaked m_{hh} distribution. Cluster 8 represents points of the parameters space with high values of κ_λ , where the main contribution to the process comes from a triangle diagram.

Figure (5) shows the m_{hh} and $|\cos\theta^*|$ distributions for all the samples considered in the 5-dimensional parameter space, grouped in thirteen clusters by the procedure described in Section (3). The clustering is clearly driven by m_{hh} variable. The impact of anomalous physics in $|\cos\theta^*|$ is expected to be small because all the different operators in our parametrization are predominantly s-wave (see for example [30]). This is evident in Fig. (5), where only few samples exhibit a non flat structure in the $|\cos\theta^*|$ variable. These correspond to points of parameters space where there is a maximal interference between the

Node	κ_λ	κ_t	c_2	c_g	c_{2g}
1	1.0	1.0	0.0	0.0	0.0
2	7.5	2.5	-0.5	0.0	0.0
3	15.0	1.5	-3.0	-0.0816	0.3010
4	5.0	2.25	3.0	0.0	0.0
5	10.0	1.5	-1.0	-0.0956	0.1240
6	1.0	0.5	4.0	-1.0	-0.3780
7	2.4	1.25	2.0	-0.2560	-0.1480
8	7.5	2.0	0.5	0.0	0.0
9	10.0	2.25	2.0	-0.2130	-0.0893
10	15.0	0.5	1.0	-0.0743	-0.0668
11	-15.0	2.0	6.0	-0.1680	-0.5180
12	2.4	2.25	2.0	-0.0616	-0.1200
13	-15.0	1.25	6.0	-0.0467	-0.5150

Table 2. Parameter values of the final benchmarks selected with $N_{clus} = 13$. The first cluster is the one that contains the SM sample.

different contributions. One of such example is the point defined by $(\kappa_\lambda = 2.4, \kappa_t = 1.0$ and $c_2 = c_g = c_{2g} = 0)$.

The $(\gamma\gamma b\bar{b})$ final state is expected to be the most sensitive to local changes in the m_{hh} spectra, however other decay channels, such as the fully leptonic $(WW b\bar{b})$ or $(b\bar{b} b\bar{b})$ could in principle to be equally sensitive to small shape variations in different regions of hard subprocess energy, especially when multi-variate analysis techniques can be implemented. With increased statistics of the analyzable data, fine structures in the kinematics -in particular in the m_{hh} distribution, *e.g.* in clusters 4, 6, and 7- will become more interesting and may call for a more specific study of the corresponding regions of parameter space.

In Fig. (6) we show the distribution of the Higgs p_T^h (which as noted *supra* is the same for both Higgs bosons at generator level) and the longitudinal momentum of the Higgs boson with the highest energy in the laboratory frame, $|p_z^h|$. Figure (5) and (6) visually confirm that the m_{hh} and $|\cos\theta^*|$ are robust to fully describe the salient features of the $2 \rightarrow 2$ process. The features shown there are more directly connected with experimental selections and acceptance cuts, and to the Higgs boson reconstruction techniques. In particular, the Higgs transverse momentum distributions allow one to gauge how the different clusters will be affected by baseline selections in the analyses targeting the corresponding benchmarks. The $|p_z^h|$ variable is highly homogeneous within each cluster, as a result of the good properties of the clustering performed using the m_{hh} variable. The full set of results up to $N_{nodes} = 20$ can be found in [61].

In Table (2) we list the parameter space points that define the chosen benchmarks. We note a tendency of the benchmark points to have $c_g \neq c_{2g} \neq 0$; this is simply a consequence of the fact the majority of the parameter space points that we investigated have these characteristics.

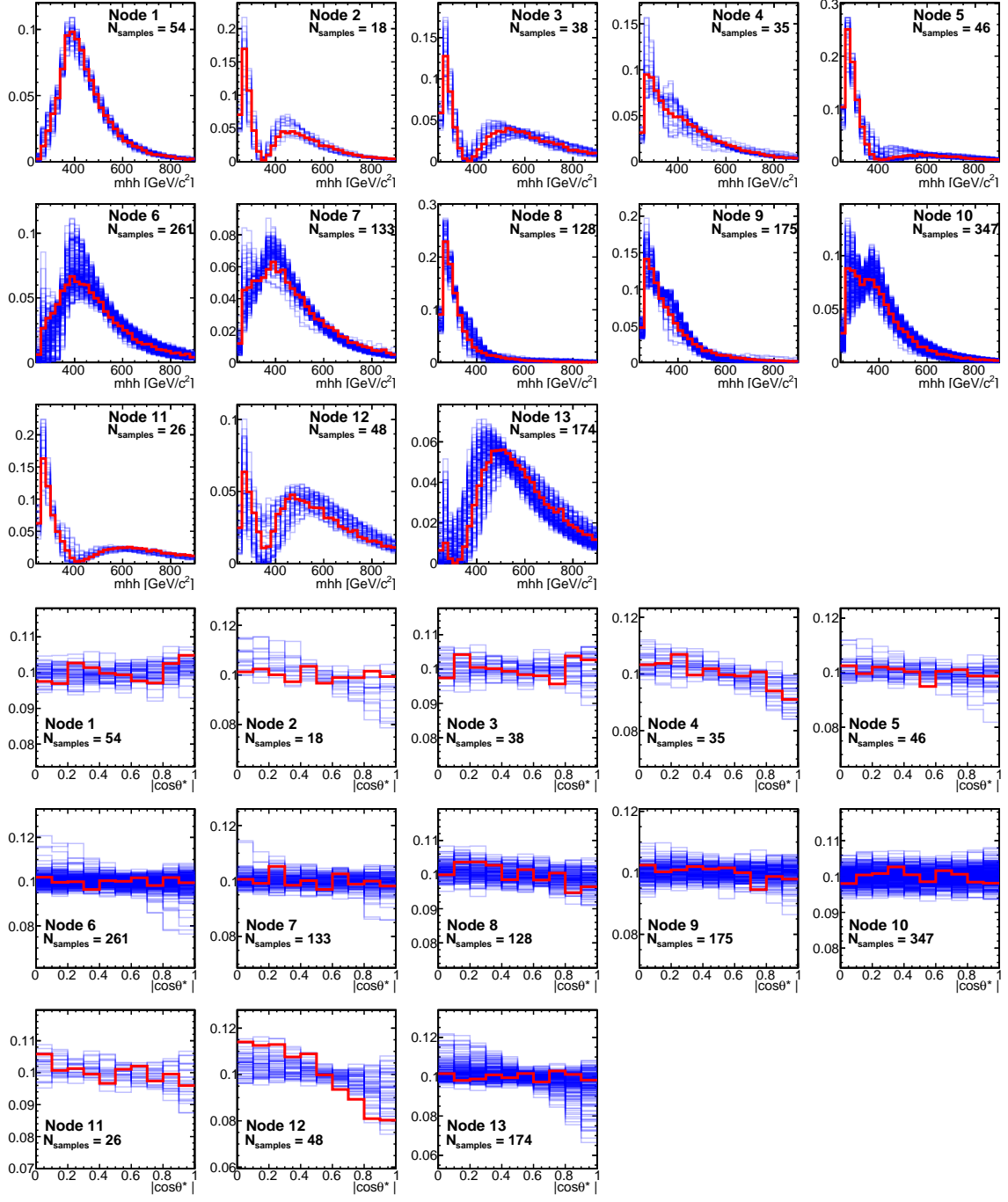


Figure 5. m_{hh} and $|\cos\theta^*|$ distributions within each cluster with $N_{clus} = 13$. The red histogram represents the benchmark point while the blue ones are the other members of the cluster. Cluster 1 contains the SM sample.

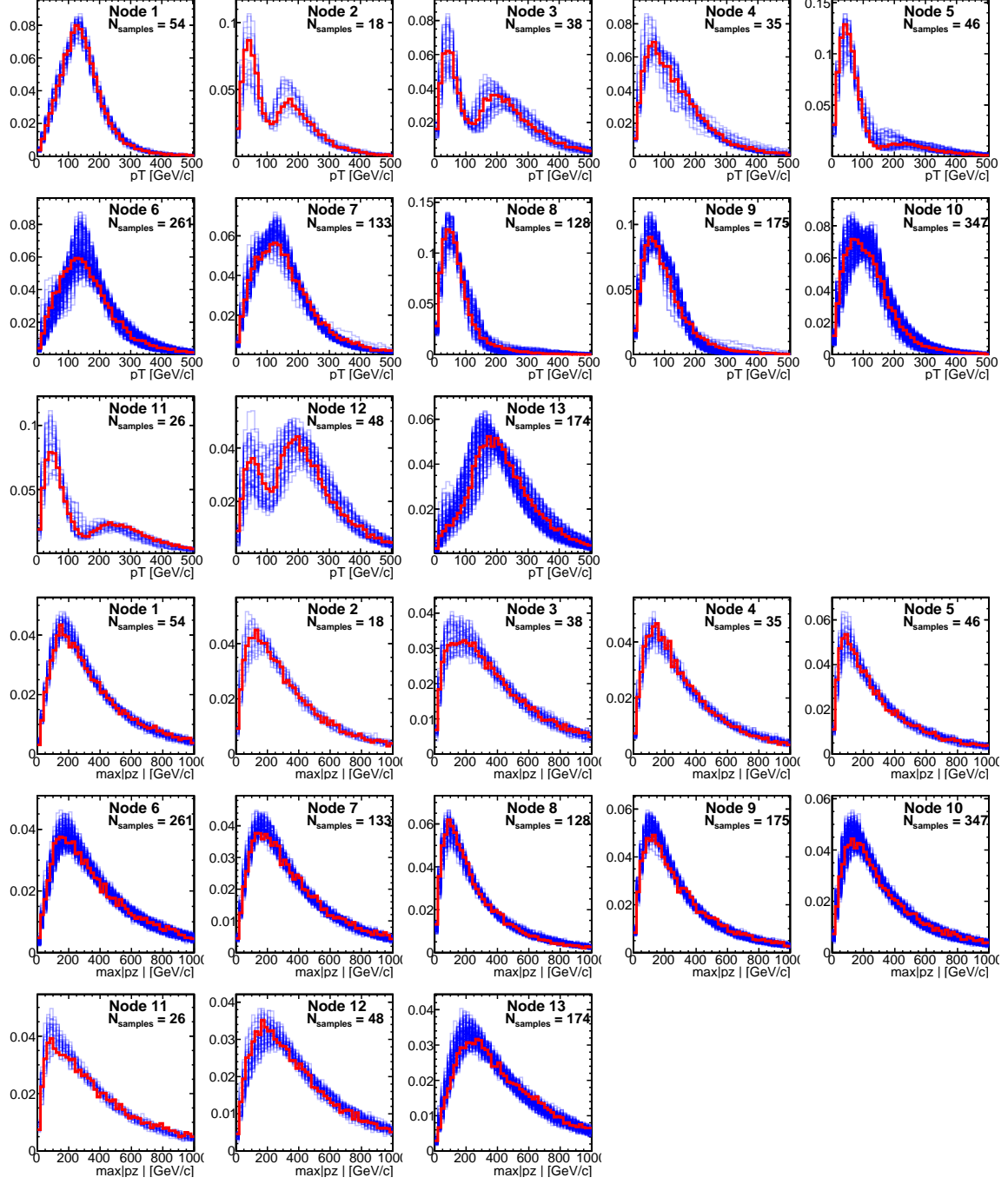


Figure 6. Generation-level Higgs p_T and $|p_z^h|$ for the choice $N_{clus} = 13$. The red distribution is the benchmark sample while the blue ones are the other members of the cluster. Cluster 1 contains the SM sample.

4.3 Maps of the Clusters in the Parameter Space

In this Section we attempt a direct mapping of the partition of the parameter space into regions which are found to produce homogeneous kinematical densities, using the choice of $N_{clus} = 13$. We organize our results in slices of parameter space, plotting the distribution of the clusters in each of them. Figure (5) shows the cluster distribution in the plane containing the SM benchmark, in particular focusing on the $\kappa_t \times \kappa_\lambda$ plane, that we will call SM-like plane, and the $\kappa_t \times c_2$ plane. The studied parameter space points are displayed following a color code. There is no logical ordering in the numbering of the clusters; we choose markers of different shape to describe how clusters spread along the different parameter space regions.

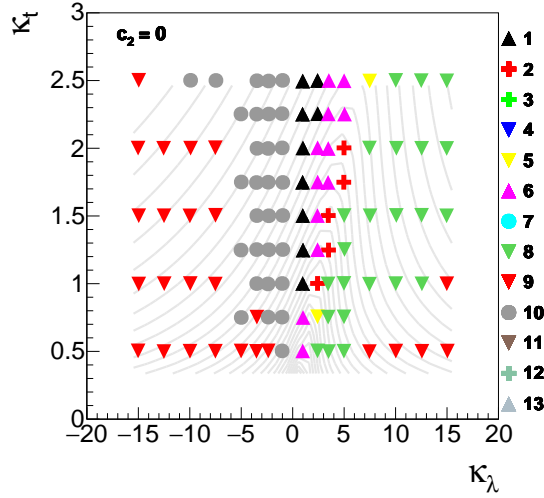


Figure 7. Distribution of nodes in the $\kappa_\lambda \times \kappa_t$ plane that contain the SM point. As indicated, triangles pointing downward symbolize clusters where the benchmark has Higgs p_T peaking at around 50 GeV or a smaller value. Circles describe clusters whose benchmark has Higgs p_T peaking around 100 GeV. Triangles pointing up describe clusters where the benchmark of the node has Higgs p_T peaking around 150 GeV or more. Finally, the crosses describe clusters that show double peaking structure in the m_{hh} distribution.

In Fig. (5) we highlight how the parameter space region around the SM benchmark in the SM-like plane is especially interesting. At LO, changes in the top Yukawa parameter as small as 30% and/or in Higgs trilinear coupling of $O(1)$ times the SM drive modifications of the differential cross section in p_T^h from single-peaked structures to more complex two-peaked shapes separated by $O(50)$ GeV. This accidental sensitivity of the kinematic behaviour to parameter values is due to the fact that the SM point is located near a cross section minimum, where there are fine cancelations between triangle and box diagrams. We come back to this specific point below. As a logical corollary of what is noted above, however, one should expect the kinematic behaviour of the SM benchmark to be quite sensitive to the accuracy of the theoretical calculation.

Figure (6) shows slices of the parameter space in the plane $\kappa_t \times c_2$ for different values of κ_λ . We observe that outside the SM-like plane there is no clear kinematic asymptotic behaviour with $|\kappa_\lambda| \gg 1$. This confirms that asymptotic approximations of the different pieces of equation (2.2) are not useful for a deep parameter space scan.

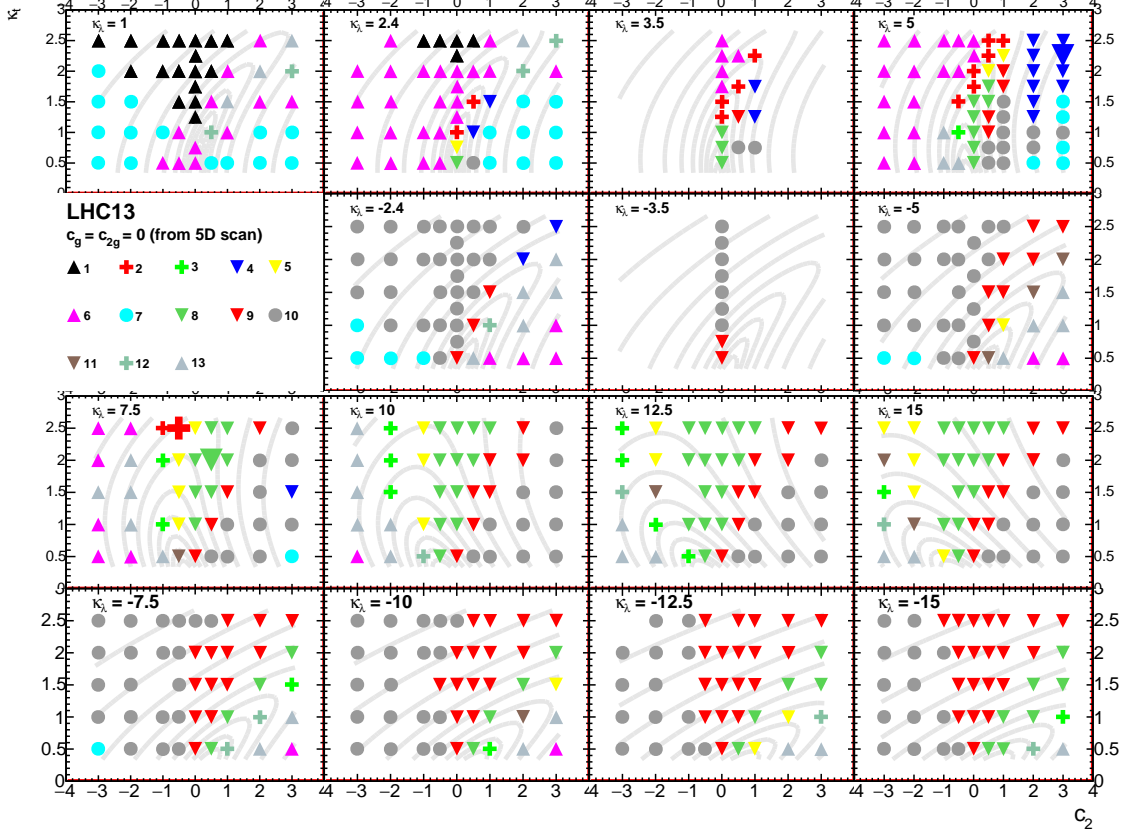


Figure 8. Distribution of nodes in the in the $c_2 \times \kappa_t$ parameters plane for different values of κ_λ when $(c_g, c_{2g}) = (0, 0)$. The different forms represent different regimes of Higgs boson p_T , as described in the caption of Fig. (7).

The above graphs suggest that the largest kinematic changes are tightly related to the minima of the cross section. If we go back to equation (2.2), we notice how all the ME pieces not related with interferences ($|M_i|^2$) are positive-defined. The minima of the cross section in each slice of parameter space are partially a reflection of regions where the interferences between the different processes are large in comparison with the other ME pieces. The correspondence however is not bilateral: the balance between the non-interference terms when navigating in the parameter space can also drive visible changes in shapes while not affecting much the total cross section.

As an additional qualitative proof of the close correspondence between the cross section minima and the regions of largest variation of the density of the kinematical distributions in the final state, we show in Fig. 10 a few maps of the cross section of di-Higgs produc-

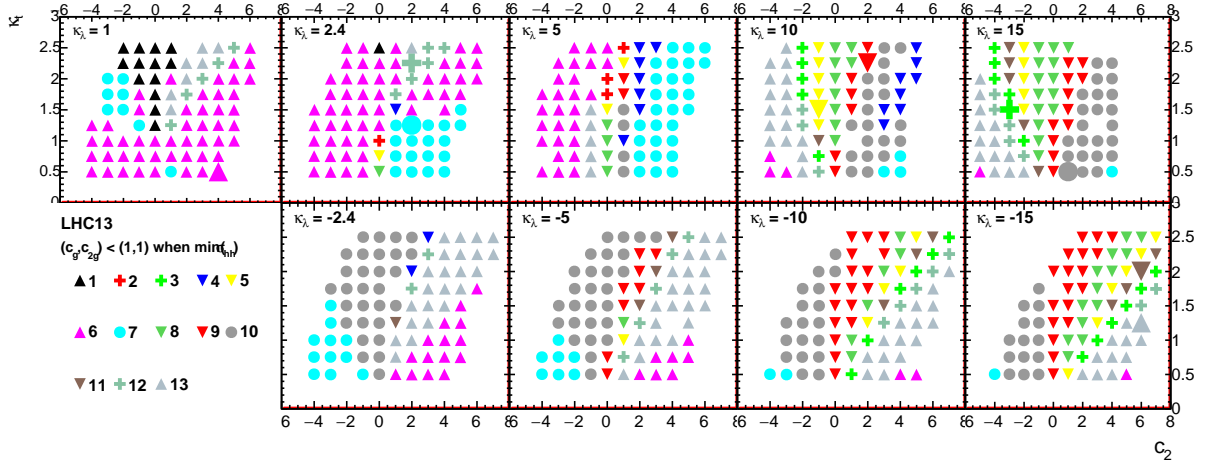


Figure 9. Distribution of clusters in the in the $c_2 \times \kappa_t$ parameter plane for different values of κ_λ and values of $(c_g, c_{2g}) < (1, 1)$ such that the di-Higgs production cross section is smaller than $100 * \sigma_{SM}$. The different shapes of the markers represent different regimes of Higgs boson p_T , as described in the caption of Fig. (7).

tion in two-dimensional subspaces of the five model parameters, with overlaid colour maps describing the magnitude of the point-to-point variations in the value of the log-likelihood test statistic defined in Section 3. The latter describe the speed with which the m_{hh} and $|\cos \theta^*|$ distributions vary, highlighting the effect of the cancelation of diagram contributions mentioned above.

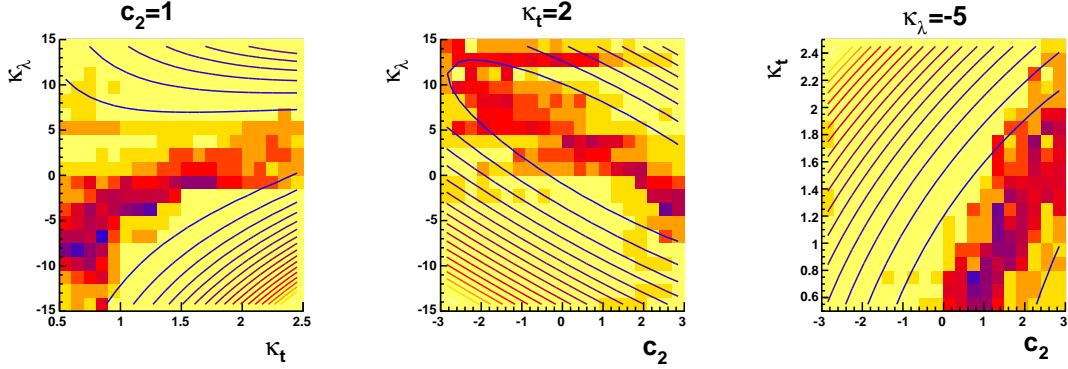


Figure 10. Superposition of isolines of cross section and colour maps of the speed at which the likelihood test statistic described in Section 3 varies as one moves around in three selected two-dimensional surfaces of the five-dimensional parameter space of BSM theories. The cross section decreases in the direction where the density of isolines decreases. Blue and red tones in the colour maps indicate the highest variation in the TS values; the colour scale is arbitrary. The behaviour observed in the graphs is common to all investigated two-dimensional planes.

5 Conclusions

The study of Higgs pair production processes at the LHC may evidence the existence of BSM physics in the form of anomalous self-couplings of the Higgs boson. While both the total Higgs pair-production cross section and the kinematics of the final state depend on those couplings, it is the latter which impacts the most the design of experimental techniques aimed at measuring the process. In this article we describe a procedure to define suitable benchmark points in the multi-dimensional parameter space spanning the possible value of the anomalous couplings. The procedure optimally chooses the benchmarks such that the study of the resulting physics has the largest impact on the exploration of the parameter space.

The technique we propose is based on the definition of a test statistic measuring the similarity of the kinematics of the Higgs pairs in the final state resulting from different parameter space points, and a suitable clustering procedure to group parameter space points together. Although it finds a very profitable application to the case of Higgs pair production at the LHC, the technique is quite general and may successfully be employed in other physics studies.

By studying gluon-fusion-initiated di-Higgs production in 13 TeV proton-proton collisions and examining the full 5-dimensional space of anomalous couplings, we find that thirteen benchmarks are sufficient to describe to a reasonable level of approximation the possible different kinematical densities that may arise from arbitrary combinations of the parameters. An experimental study which focuses on those thirteen scenarios is guaranteed to explore the parameter space without leaving unexplored “holes”.

Acknowledgments

We wish to thank Maxime Gouzevich, Olivier Bondu, Fabio Maltoni, Eleni Vryonidou and Andreas Papaefstathiou, Jose Zurita for useful discussions. A.O would like to extend this list to Andrea Wulzer, Giuliano Panico and Christoph Englert. We also thank Amina Zghiche, Debdeep Ghosal and Serguei Ganjour for further cross checks. A.O. and F.G. would like to express special thanks to the Mainz Institute for Theoretical Physics (MITP) for its hospitality. A.O. is supported by MIURFIRB grant RBFR12H1MW grant. The research of F.G is supported by a Marie Curie Intra European Fellowship within the 7th European Community Framework Programme (grant no. PIEF-GA-2013-628224).

References

- [1] Georges Aad et al. “Observation of a new particle in the search for the Standard Model Higgs boson with the ATLAS detector at the LHC”. In: *Phys.Lett.* B716 (2012), pp. 1–29. DOI: [10.1016/j.physletb.2012.08.020](https://doi.org/10.1016/j.physletb.2012.08.020). arXiv:[1207.7214](https://arxiv.org/abs/1207.7214) [hep-ex].
- [2] Serguei Chatrchyan et al. “Observation of a new boson at a mass of 125 GeV with the CMS experiment at the LHC”. In: *Phys.Lett.* B716 (2012), pp. 30–61. DOI: [10.1016/j.physletb.2012.08.021](https://doi.org/10.1016/j.physletb.2012.08.021). arXiv:[1207.7235](https://arxiv.org/abs/1207.7235) [hep-ex].

- [3] E.W. Nigel Glover and J.J. van der Bij. “Higgs Boson Pair Production via Gluon Fusion”. In: *Nucl.Phys.* B309 (1988), p. 282. DOI: [10.1016/0550-3213\(88\)90083-1](#).
- [4] Aleksandr Azatov, Roberto Contino, Giuliano Panico, and Minho Son. “Effective field theory analysis of double Higgs production via gluon fusion”. In: (2015). arXiv:[1502.00539 \[hep-ph\]](#).
- [5] Magdalena Slawinska, Wouter van den Wollenberg, Bob van Eijk, and Stan Bentvelsen. “Phenomenology of the trilinear Higgs coupling at proton-proton colliders”. In: (2014). arXiv:[1408.5010 \[hep-ph\]](#).
- [6] Vernon Barger, Lisa L. Everett, C.B. Jackson, and Gabe Shaughnessy. “Higgs-Pair Production and Measurement of the Triscalar Coupling at LHC(8,14)”. In: *Phys.Lett.* B728 (2014), pp. 433–436. DOI: [10.1016/j.physletb.2013.12.013](#). arXiv:[1311.2931 \[hep-ph\]](#).
- [7] Alan J. Barr, Matthew J. Dolan, Christoph Englert, Danilo Enoque Ferreira de Lima, and Michael Spannowsky. “Higgs Self-Coupling Measurements at a 100 TeV Hadron Collider”. In: *JHEP* 1502 (2015), p. 016. DOI: [10.1007/JHEP02\(2015\)016](#). arXiv:[1412.7154 \[hep-ph\]](#).
- [8] Ning Liu, Songlin Hu, Bingfang Yang, and Jinzhong Han. “Impact of top-Higgs couplings on Di-Higgs production at future colliders”. In: *JHEP* 1501 (2015), p. 008. DOI: [10.1007/JHEP01\(2015\)008](#). arXiv:[1408.4191 \[hep-ph\]](#).
- [9] Florian Goertz, Andreas Papaefstathiou, Li Lin Yang, and JosÃl Zurita. “Higgs boson pair production in the D=6 extension of the SM”. In: (2014). arXiv:[1410.3471 \[hep-ph\]](#).
- [10] Chuan-Ren Chen and Ian Low. “Double take on new physics in double Higgs boson production”. In: *Phys.Rev.* D90.1 (2014), p. 013018. DOI: [10.1103/PhysRevD.90.013018](#). arXiv:[1405.7040 \[hep-ph\]](#).
- [11] Matthew J. Dolan, Christoph Englert, and Michael Spannowsky. “New Physics in LHC Higgs boson pair production”. In: *Phys.Rev.* D87.5 (2013), p. 055002. DOI: [10.1103/PhysRevD.87.055002](#). arXiv:[1210.8166 \[hep-ph\]](#).
- [12] Florian Goertz, Andreas Papaefstathiou, Li Lin Yang, and Jose Zurita. “Higgs Boson self-coupling measurements using ratios of cross sections”. In: *JHEP* 1306 (2013), p. 016. DOI: [10.1007/JHEP06\(2013\)016](#). arXiv:[1301.3492 \[hep-ph\]](#).
- [13] Kenji Nishiwaki, Saurabh Niyogi, and Ambresh Shivaji. “ ttH Anomalous Coupling in Double Higgs Production”. In: *JHEP* 1404 (2014), p. 011. DOI: [10.1007/JHEP04\(2014\)011](#). arXiv:[1309.6907 \[hep-ph\]](#).
- [14] Weiming Yao. “Studies of measuring Higgs self-coupling with $HH \rightarrow b\bar{b}\gamma\gamma$ at the future hadron colliders”. In: (2013). arXiv:[1308.6302 \[hep-ph\]](#).
- [15] Ding Yu Shao, Chong Sheng Li, Hai Tao Li, and Jian Wang. “Threshold resummation effects in Higgs boson pair production at the LHC”. In: *JHEP* 1307 (2013), p. 169. DOI: [10.1007/JHEP07\(2013\)169](#). arXiv:[1301.1245 \[hep-ph\]](#).

- [16] David Wardrope, Eric Jansen, Nikos Konstantinidis, Ben Cooper, Rebecca Falla, et al. “Non-resonant Higgs pair production in the $b\bar{b}b\bar{b}$ final state at the LHC”. In: (2014). arXiv:[1410.2794 \[hep-ph\]](#).
- [17] Matthew J. Dolan, Christoph Englert, Nicolas Greiner, Karl Nordstrom, and Michael Spannowsky. “ $hhjj$ production at the LHC”. In: (2015). arXiv:[1506.08008 \[hep-ph\]](#).
- [18] Hong-Jian He, Jing Ren, and Weiming Yao. “Probing New Physics of Cubic Higgs Interaction via Higgs Pair Production at Hadron Colliders”. In: (2015). arXiv:[1506.03302 \[hep-ph\]](#).
- [19] Chih-Ting Lu, Jung Chang, Kingman Cheung, and Jae Sik Lee. “A Model Independent Analysis of Higgs-boson pair production at the LHC”. In: (2015). arXiv:[1505.00957 \[hep-ph\]](#).
- [20] V. Hankele, G. Klamke, D. Zeppenfeld, and T. Figy. “Anomalous Higgs boson couplings in vector boson fusion at the CERN LHC”. In: *Phys.Rev.* D74 (2006), p. 095001. DOI: [10.1103/PhysRevD.74.095001](#). arXiv:[hep-ph/0609075 \[hep-ph\]](#).
- [21] Olivier Bondu, Rogerio Rosenfeld, Veronica Sanz, Alexander Belyaev, Andrea Mas-sironi, and Alexandra Oliveira. “Resonant Higgs Pair Production in Vector Boson Fusion at the LHC with di-higgs final states.” Les Houches 2013 proceedings - To be published.
- [22] Christoph Englert, Frank Krauss, Michael Spannowsky, and Jennifer Thompson. “Di-Higgs phenomenology in $t\bar{t}hh$: The forgotten channel”. In: *Phys.Lett.* B743 (2015), pp. 93–97. DOI: [10.1016/j.physletb.2015.02.041](#). arXiv:[1409.8074 \[hep-ph\]](#).
- [23] Vardan Khachatryan et al. “Precise determination of the mass of the Higgs boson and tests of compatibility of its couplings with the standard model predictions using proton collisions at 7 and 8 TeV”. In: (2014). arXiv:[1412.8662 \[hep-ex\]](#).
- [24] ATLAS Collaboration. *Measurements of the Higgs boson production and decay rates and coupling strengths using pp collision data at $\sqrt{s} = 7$ and 8 TeV in the ATLAS experiment*. Tech. rep. ATLAS-CONF-2015-007. Geneva: CERN, 2015. URL: <http://cds.cern.ch/record/2002212>.
- [25] Florian Goertz. “Indirect Handle on the Down-Quark Yukawa Coupling”. In: *Phys.Rev.Lett.* 113.26 (2014), p. 261803. DOI: [10.1103/PhysRevLett.113.261803](#). arXiv:[1406.0102 \[hep-ph\]](#).
- [26] G.F. Giudice, C. Grojean, A. Pomarol, and R. Rattazzi. “The Strongly-Interacting Light Higgs”. In: *JHEP* 0706 (2007), p. 045. DOI: [10.1088/1126-6708/2007/06/045](#). arXiv:[hep-ph/0703164 \[hep-ph\]](#).
- [27] W. Buchmuller and D. Wyler. “Effective Lagrangian Analysis of New Interactions and Flavor Conservation”. In: *Nucl.Phys.* B268 (1986), pp. 621–653. DOI: [10.1016/0550-3213\(86\)90262-2](#).
- [28] Roberto Contino, Margherita Ghezzi, Christophe Grojean, Margarete Muhlleitner, and Michael Spira. “Effective Lagrangian for a light Higgs-like scalar”. In: *JHEP* 1307 (2013), p. 035. DOI: [10.1007/JHEP07\(2013\)035](#). arXiv:[1303.3876 \[hep-ph\]](#).

- [29] M. Gillioz, R. Grober, C. Grojean, M. Muhlleitner, and E. Salvioni. “Higgs Low-Energy Theorem (and its corrections) in Composite Models”. In: *JHEP* 1210 (2012), p. 004. DOI: [10.1007/JHEP10\(2012\)004](https://doi.org/10.1007/JHEP10(2012)004). arXiv:[1206.7120](https://arxiv.org/abs/1206.7120) [[hep-ph](#)].
- [30] T. Plehn, M. Spira, and P.M. Zerwas. “Pair production of neutral Higgs particles in gluon-gluon collisions”. In: *Nucl.Phys.* B479 (1996), pp. 46–64. DOI: [10.1016/0550-3213\(96\)00418-X](https://doi.org/10.1016/0550-3213(96)00418-X). arXiv:[hep-ph/9603205](https://arxiv.org/abs/hep-ph/9603205) [[hep-ph](#)].
- [31] A. Belyaev, Manuel Drees, Oscar J.P. Eboli, J.K. Mizukoshi, and S.F. Novaes. “Supersymmetric Higgs pair discovery prospects at hadron colliders”. In: (1999), pp. 748–751. arXiv:[hep-ph/9910400](https://arxiv.org/abs/hep-ph/9910400) [[hep-ph](#)].
- [32] Michael Spira and James D. Wells. “Higgs bosons strongly coupled to the top quark”. In: *Nucl.Phys.* B523 (1998), pp. 3–16. DOI: [10.1016/S0550-3213\(98\)00107-2](https://doi.org/10.1016/S0550-3213(98)00107-2). arXiv:[hep-ph/9711410](https://arxiv.org/abs/hep-ph/9711410) [[hep-ph](#)].
- [33] Chengcheng Han, Xuanning Ji, Lei Wu, Peiwen Wu, and Jin Min Yang. “Higgs pair production with SUSY QCD correction: revisited under current experimental constraints”. In: *JHEP* 1404 (2014), p. 003. DOI: [10.1007/JHEP04\(2014\)003](https://doi.org/10.1007/JHEP04(2014)003). arXiv:[1307.3790](https://arxiv.org/abs/1307.3790) [[hep-ph](#)].
- [34] Michael J. Dugan, Howard Georgi, and David B. Kaplan. “Anatomy of a Composite Higgs Model”. In: *Nucl.Phys.* B254 (1985), p. 299. DOI: [10.1016/0550-3213\(85\)90221-4](https://doi.org/10.1016/0550-3213(85)90221-4).
- [35] Adam Falkowski and Francesco Riva. “Model-independent precision constraints on dimension-6 operators”. In: *JHEP* 1502 (2015), p. 039. DOI: [10.1007/JHEP02\(2015\)039](https://doi.org/10.1007/JHEP02(2015)039). arXiv:[1411.0669](https://arxiv.org/abs/1411.0669) [[hep-ph](#)].
- [36] Adam Falkowski. “Effective field theory approach to LHC Higgs data”. In: (2015). arXiv:[1505.00046](https://arxiv.org/abs/1505.00046) [[hep-ph](#)].
- [37] Michael Duehrssen-Debling, Andre Tinoco Mendes, Adam Falkowski, and Gino Isidori. “Higgs Basis: Proposal for an EFT basis choice for LHC HXSWG”. In: (2015). URL: <https://cds.cern.ch/record/2001958>.
- [38] Benjamin Fuks, Fabio Maltoni, Kentarou Mawatari, Ken Mimasu, and Veronica Sanz. “<https://github.com/kenmimasu/Rosetta> ”.
- [39] P. Artoisenet, P. de Aquino, F. Demartin, R. Frederix, S. Frixione, et al. “A framework for Higgs characterisation”. In: *JHEP* 1311 (2013), p. 043. DOI: [10.1007/JHEP11\(2013\)043](https://doi.org/10.1007/JHEP11(2013)043). arXiv:[1306.6464](https://arxiv.org/abs/1306.6464) [[hep-ph](#)].
- [40] Beranger Dumont, Sylvain Fichet, and Gero von Gersdorff. “A Bayesian view of the Higgs sector with higher dimensional operators”. In: *JHEP* 1307 (2013), p. 065. DOI: [10.1007/JHEP07\(2013\)065](https://doi.org/10.1007/JHEP07(2013)065). arXiv:[1304.3369](https://arxiv.org/abs/1304.3369) [[hep-ph](#)].
- [41] J. Elias-Miro, J.R. Espinosa, E. Masso, and A. Pomarol. “Higgs windows to new physics through d=6 operators: constraints and one-loop anomalous dimensions”. In: *JHEP* 1311 (2013), p. 066. DOI: [10.1007/JHEP11\(2013\)066](https://doi.org/10.1007/JHEP11(2013)066). arXiv:[1308.1879](https://arxiv.org/abs/1308.1879) [[hep-ph](#)].

- [42] Alex Pomarol and Francesco Riva. “Towards the Ultimate SM Fit to Close in on Higgs Physics”. In: *JHEP* 1401 (2014), p. 151. DOI: [10.1007/JHEP01\(2014\)151](#). arXiv:[1308.2803 \[hep-ph\]](#).
- [43] Rick S. Gupta, Alex Pomarol, and Francesco Riva. “BSM Primary Effects”. In: *Phys.Rev.* D91.3 (2015), p. 035001. DOI: [10.1103/PhysRevD.91.035001](#). arXiv:[1405.0181 \[hep-ph\]](#).
- [44] G. Aad et al. “Search For Higgs Boson Pair Production in the $\gamma\gamma b\bar{b}$ Final State using pp Collision Data at $\sqrt{s} = 8$ TeV from the ATLAS Detector”. In: *Phys.Rev.Lett.* 114.8 (2015), p. 081802. DOI: [10.1103/PhysRevLett.114.081802](#). arXiv:[1406.5053 \[hep-ex\]](#).
- [45] Daniel de Florian and Javier Mazzitelli. “Next-to-Next-to-Leading Order QCD Corrections to Higgs Boson Pair Production”. In: *PoS LL2014* (2014), p. 029. arXiv:[1405.4704 \[hep-ph\]](#).
- [46] Jonathan Grigo, Kirill Melnikov, and Matthias Steinhauser. “Virtual corrections to Higgs boson pair production in the large top quark mass limit”. In: *Nucl.Phys.* B888 (2014), pp. 17–29. DOI: [10.1016/j.nuclphysb.2014.09.003](#). arXiv:[1408.2422 \[hep-ph\]](#).
- [47] Jun Gao, Marco Guzzi, Joey Huston, Hung-Liang Lai, Zhao Li, et al. “CT10 next-to-next-to-leading order global analysis of QCD”. In: *Phys.Rev.* D89.3 (2014), p. 033009. DOI: [10.1103/PhysRevD.89.033009](#). arXiv:[1302.6246 \[hep-ph\]](#).
- [48] R. Frederix, S. Frixione, V. Hirschi, F. Maltoni, O. Mattelaer, et al. “Higgs pair production at the LHC with NLO and parton-shower effects”. In: *Phys.Lett.* B732 (2014), pp. 142–149. DOI: [10.1016/j.physletb.2014.03.026](#). arXiv:[1401.7340 \[hep-ph\]](#).
- [49] Daniel de Florian and Javier Mazzitelli. “Higgs pair production at next-to-next-to-leading logarithmic accuracy at the LHC”. In: (2015). arXiv:[1505.07122 \[hep-ph\]](#).
- [50] F. Maltoni, E. Vryonidou, and M. Zaro. “Top-quark mass effects in double and triple Higgs production in gluon-gluon fusion at NLO”. In: *JHEP* 1411 (2014), p. 079. DOI: [10.1007/JHEP11\(2014\)079](#). arXiv:[1408.6542 \[hep-ph\]](#).
- [51] Ramona Grober, Margarete Muhlleitner, Michael Spira, and Juraj Streicher. “NLO QCD Corrections to Higgs Pair Production including Dimension-6 Operators”. In: (2015). arXiv:[1504.06577 \[hep-ph\]](#).
- [52] Georges Aad et al. “Search for Higgs boson pair production in the $b\bar{b}b\bar{b}$ final state from pp collisions at $\sqrt{s} = 8$ TeV with the ATLAS detector”. In: (2015). arXiv:[1506.00285 \[hep-ex\]](#).
- [53] Benoit Hespel, David Lopez-Val, and Eleni Vryonidou. “Higgs pair production via gluon fusion in the Two-Higgs-Doublet Model”. In: *JHEP* 1409 (2014), p. 124. DOI: [10.1007/JHEP09\(2014\)124](#). arXiv:[1407.0281 \[hep-ph\]](#).

- [54] Stefano Frixione, Fabian Stoeckli, Paolo Torrielli, and Bryan R. Webber. “NLO QCD corrections in Herwig++ with MC@NLO”. In: *JHEP* 1101 (2011), p. 053. DOI: [10.1007/JHEP01\(2011\)053](https://doi.org/10.1007/JHEP01(2011)053). arXiv:[1010.0568](https://arxiv.org/abs/1010.0568) [[hep-ph](#)].
- [55] J. Alwall, R. Frederix, S. Frixione, V. Hirschi, F. Maltoni, et al. “The automated computation of tree-level and next-to-leading order differential cross sections, and their matching to parton shower simulations”. In: *JHEP* 1407 (2014), p. 079. DOI: [10.1007/JHEP07\(2014\)079](https://doi.org/10.1007/JHEP07(2014)079). arXiv:[1405.0301](https://arxiv.org/abs/1405.0301) [[hep-ph](#)].
- [56] Richard D. Ball et al. “Precision determination of electroweak parameters and the strange content of the proton from neutrino deep-inelastic scattering”. In: *Nucl.Phys.* B823 (2009), pp. 195–233. DOI: [10.1016/j.nuclphysb.2009.08.003](https://doi.org/10.1016/j.nuclphysb.2009.08.003). arXiv:[0906.1958](https://arxiv.org/abs/0906.1958) [[hep-ph](#)].
- [57] John C. Collins and Davison E. Soper. “Angular distribution of dileptons in high-energy hadron collisions”. In: *Phys. Rev. D* 16 (7 1977), pp. 2219–2225. DOI: [10.1103/PhysRevD.16.2219](https://doi.org/10.1103/PhysRevD.16.2219). URL: <http://link.aps.org/doi/10.1103/PhysRevD.16.2219>.
- [58] B. Aslan and Gunter Zech. “A New class of binning free, multivariate goodness of fit tests: The Energy tests”. In: (2002). arXiv:[hep-ex/0203010](https://arxiv.org/abs/hep-ex/0203010) [[hep-ex](#)].
- [59] Steve Baker and Robert D. Cousins. “Clarification of the Use of Chi Square and Likelihood Functions in Fits to Histograms”. In: *Nucl. Instr. Meth.* 221 (1984), pp. 437–442.
- [60] S.S. Wilks. “The Large-Sample Distribution of the Likelihood Ratio for Testing Composite Hypotheses”. In: *Annals Math.Statist.* 9.1 (1938), pp. 60–62. DOI: [10.1214/aoms/1177732360](https://doi.org/10.1214/aoms/1177732360).
- [61] “ <https://twiki.cern.ch/twiki/bin/view/Sandbox/NonResonantHHatLHC> ”. Twiki with the full set of results.